












RESEARCH ARTICLE

Structural, compositional, and functional effects of blunt and sharp cartilage damage on the joint: A 9-month equine groove model study

Nikae C. R. te Moller¹  | Ali Mohammadi²  | Saskia Plomp¹ |
Filipe M. Serra Bragança¹  | Martijn Beukers¹  | Behdad Pouran⁴ |
Isaac O. Afara²  | Ervin Nippolainen²  | Janne T. A. Mäkelä²  |
Rami K. Korhonen²  | Juha Töyräs^{2,3,5}  | Harold Brommer¹  |
P. René van Weeren¹ 

¹Department of Clinical Sciences, Faculty of Veterinary Medicine, Utrecht University, Utrecht, the Netherlands

²Department of Applied Physics, University of Eastern Finland, Kuopio, Finland

³Diagnostic Imaging Center, Kuopio University Hospital, Kuopio, Finland

⁴Department of Orthopaedics, University Medical Center Utrecht, Utrecht, the Netherlands

⁵School of Information Technology and Electrical Engineering, The University of Queensland, Brisbane, Queensland, Australia

Correspondence

Nikae C. R. te Moller, Department of Clinical Sciences, Faculty of Veterinary Medicine, Utrecht University, Yalelaan 114, 3584 CM Utrecht, the Netherlands.
Email: n.c.r.temoller@uu.nl

Funding information

ReumaNederland, Grant/Award Number: LLP-22; Nederlandse Organisatie voor Wetenschappelijk Onderzoek, Grant/Award Number: 022.005.018; University of Eastern Finland's Doctoral Programme in Science, Technology and Computing (SCITECO); Academy of Finland, Grant/Award Numbers: 324529, 307932

Abstract

This study aimed to quantify the long-term progression of blunt and sharp cartilage defects and their effect on joint homeostasis and function of the equine carpus. In nine adult Shetland ponies, the cartilage in the radiocarpal and middle carpal joint of one front limb was grooved (blunt or sharp randomized). The ponies were subjected to an 8-week exercise protocol and euthanized at 39 weeks. Structural and compositional alterations in joint tissues were evaluated *in vivo* using serial radiographs, synovial biopsies, and synovial fluid samples. Joint function was monitored by quantitative gait analysis. Macroscopic, microscopic, and biomechanical evaluation of the cartilage and assessment of subchondral bone parameters were performed *ex vivo*. Grooved cartilage showed higher OARSI microscopy scores than the contralateral sham-operated controls ($p < 0.0001$). Blunt-grooved cartilage scored higher than sharp-grooved cartilage ($p = 0.007$) and fixed charge density around these grooves was lower ($p = 0.006$). Equilibrium and instantaneous moduli trended lower in grooved cartilage than their controls (significant for radiocarpal joints). Changes in other tissues included a threefold to sevenfold change in interleukin-6 expression in synovium from grooved joints at week 23 ($p = 0.042$) and an increased CII/C2C ratio in synovial fluid extracted from blunt-grooved joints at week 35 ($p = 0.010$). Gait analysis outcome revealed mild, gradually increasing lameness. In conclusion, blunt and, to a lesser extent, sharp grooves in combination with a period of moderate exercise, lead to mild degeneration in equine carpal cartilage over a 9-month period, but the effect on overall joint health remains limited.

KEYWORDS

articular cartilage, chondral defect model, horse, multiple modality monitoring, osteoarthritis

This is an open access article under the terms of the Creative Commons Attribution-NonCommercial-NoDerivs License, which permits use and distribution in any medium, provided the original work is properly cited, the use is non-commercial and no modifications or adaptations are made.

© 2020 The Authors. *Journal of Orthopaedic Research*® published by Wiley Periodicals LLC on behalf of Orthopaedic Research Society.

1 | INTRODUCTION

Osteoarthritis (OA) affects millions of people worldwide and is also a common burden in animals. Particularly in the horse industry, the high incidence of OA is an important concern.¹ The close similarity between equine and human articular cartilage and the horse being a target species in itself, make equine models very useful for studying early pathobiological events of OA.^{2,3}

Recently, the articular groove model that was earlier used in dogs, sheep, and rats,⁴⁻⁶ was applied in the equine metacarpophalangeal (MCP) joint.⁷ In that study the cartilage was surgically grooved onto the calcified cartilage layer and the animals were subjected to moderate physical exercise. In a 10-week pilot study in Shetland ponies, we showed later that the model behaved similarly in middle carpal and MCP joints.⁸

The cited studies focused on structural changes of cartilage and subchondral bone, biochemical analysis of cartilage, and, to some extent, synovial fluid (SF) biomarkers.⁴⁻⁷ Data on biomechanical changes of the cartilage is still limited, despite the growing awareness of the crucial role of biomechanics in our current incapacity to regenerate functional articular cartilage.⁹ In this context, the responses to various types of lesions that differently affect the native architecture of the cartilage is of interest. In the 1960s, the scarification model (a groove model with sharp cuts) was used in rabbits¹⁰ and the response of articular cartilage to blunt grooves versus sharp cuts has been investigated *in vitro*,¹¹ but no *in vivo* comparison has been made. Also, longitudinal information on the progress of chondral grooves is sparse. This kind of data would be valuable for the validation of computational models aiming to predict the progression of focal defects and ensuing posttraumatic OA.¹² Better insights in early-stage processes could help timely recognition of (the risk to develop) OA and may reveal new treatment targets.

This study aimed at quantifying the long-term progression of artificially created cartilage grooves and their effect on other joint tissues in the equine carpal joint by monitoring changes at a structural, compositional, and functional level *in vivo* and *ex vivo*. We hypothesized that 1) damage to articular cartilage would always lead to progressive degeneration, but that substantial disruption of the matrix ("blunt grooves") would accelerate this process compared with more subtle damage ("sharp grooves") and that 2) progressive cartilage degeneration would affect joint homeostasis, evidenced by alterations in other joint tissues and functionally as changes in gait pattern.

2 | METHODS

2.1 | Animals

The study included nine healthy adult female Shetland ponies (mean \pm SD) age 6.8 ± 2.6 years (range 4–13 years); mean \pm SD bodyweight 203 ± 15.3 kg (range 171–220 kg); details of sample size calculation in Supporting Information text S1). The ponies were not lame and did not suffer from lateral patellar subluxation or upward patellar fixation

(well-known disorders in this breed). The study was authorized by the Utrecht University Animal Experiments Committee and the Central Committee for Animal Experiments (permit AVD108002015307) in compliance with the Dutch Act on Animal Experimentation. Animal care was performed in accordance with the Utrecht University guidelines.

2.2 | Surgical procedures

All surgeries were performed under general anesthesia (details of procedure in Supporting Information Text S2). Grooves were created by a board-certified equine surgeon (HB) in one randomly assigned front limb per animal. In the cartilage layer of the radial facet of the third carpal bone and of the dorsoproximal surface of the intermediate carpal bone, three grooves (two running in parallel in palmarodorsal direction and one in mediolateral direction) were made via arthrotomy of the middle carpal and radiocarpal joint, respectively (Figure 1A). Blunt and sharp grooves were randomly assigned to either of the two joints ($n = 9$ per groove type). Blunt grooves were made using a hooked arthroscopic probe with a sharpened tip (Figure 1B), sharp grooves with a surgical blade (Beaver Mini-Blade®, MFID: 376400) clamped in a custom-made device (Figure 1C). The contralateral joints were sham-operated and served as controls ($n = 18$). After surgery, ponies were kept for 3 weeks in individual boxes allowing mutual contact.

2.3 | Exercise program

The ponies were accustomed to treadmill (Mustang 200; Kagra AG) exercise 3 weeks before surgery. After initial box-rest, they were hand-walked daily for 15 min 2 weeks post-surgery. After 3 weeks, they were moved to an open group shed (approx. 125 m²) and subjected to an incremental exercise protocol for 8 weeks (Table 1). After 26 weeks, the ponies were allowed free pasture exercise until the end of the study.

2.4 | In vivo monitoring and post-mortem analysis

Structural and compositional changes in the joints were monitored through serial radiographs, synovial biopsies, and SF samples. Joint function was monitored by quantitative gait analysis (Figure 2A). At 39 weeks, the ponies were euthanized (Supporting Information Text S2). Grooved and control joints were harvested and stored at -20°C until post-mortem analyses focusing at macroscopic and microscopic cartilage degeneration (primary outcomes), cartilage biomechanics, and subchondral bone parameters (Figure 2B).

2.5 | Macroscopic examination of cartilage

Joints were thawed overnight at 4°C , and joint surfaces were photographed for macroscopic evaluation using a 0-4 scale.¹³

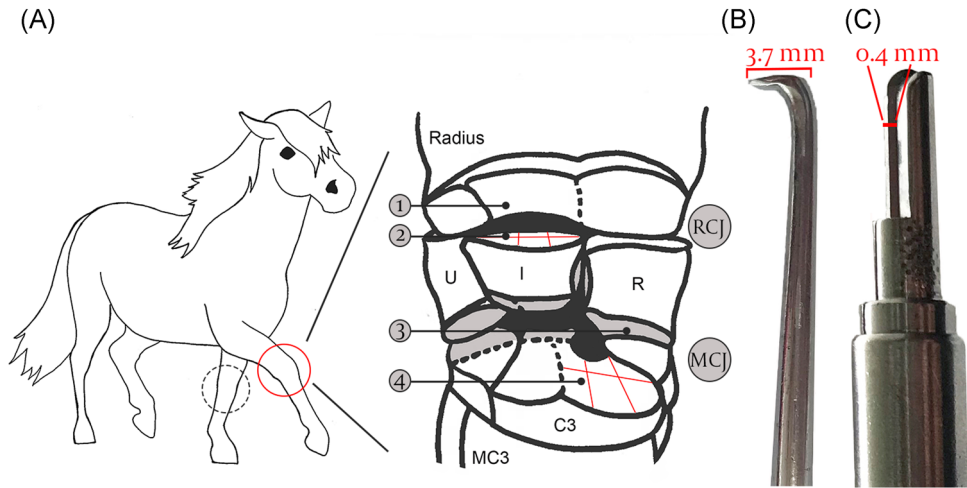


FIGURE 1 (A) The carpal groove model shown for the right carpus, with the left carpus representing the sham-operated control. C3, third carpal bone; I, intermediate carpal bone; MC3, third metacarpal bone; MCJ, middle carpal joint; R, radial carpal bone, RCJ, radiocarpal joint; U, ulnar carpal bone. Grooves were created at the dorsoproximal surface of the intermediate carpal bone (2) and at the radial facet of the proximal surface of the third carpal bone (4); one blunt, one sharp, randomly chosen. 1, distal surface of the radius (kissing site), 3, distal surface of the radial carpal bone (kissing site). (B) An arthroscopic probe with a sharpened tip was used to create blunt grooves. (C) A surgical mini blade clamped in a custom-made device was used to create sharp grooves [Color figure can be viewed at wileyonlinelibrary.com]

The actual grooves were excluded from this grading scheme. Photographs were blind-coded and randomly scored twice with one week in between by two observers (NM, HB). Osteochondral samples from the grooved sites and the contact sites (“kissing sites”), and their contralateral controls were harvested using an oscillating saw (multitool PMF 220CE; Bosch) and stored at -20°C .

2.6 | Micro-computed tomography (CT) imaging of osteochondral samples

Samples were thawed at room temperature before high-resolution micro-CT imaging (Quantum FX®; Perkin Elmer) and subsequently stored at -20°C (Supporting Information Text S3). Trabecular bone thickness and trabecular bone volume fraction

TABLE 1 Training protocol (weeks after groove surgery)

Week	Day	Treadmill (min/gait)						Horse walker (min/day)		
		Walk	Trot	Canter	Walk	Canter	Trot	Walk	Total	Walk
3	Mo-Fri	10	-	-	-	-	-	-	10	-
4	Mo	3	2	-	2	-	2	5	14	15
	Tue	3	3	-	2	-	3	5	16	
	Thu	3	3	-	2	-	3	5	16	
	Fri	3	4	-	2	-	4	5	18	
5	Mo	3	5	-	2	-	5	5	20	30
	Tue	3	4	1	1	1	2	5	17	
	We	5	4	1	1	1	2	5	19	
	Thu	3	5	-	2	-	2	5	17	
	Fri	5	4	2	-	-	2	5	18	
6-11	Mo	3	5	-	2	-	5	5	20	30
	Tue	5	4	2	-	-	2	5	18	
	Thu	3	5	-	2	-	5	5	20	
	Fri	5	4	2	-	-	2	5	18	

Note: Speed at walk, trot, and canter was set at 4.5, 11, and 21 km/h, respectively. Walking exercise in the horse walker was performed 7 days/week.

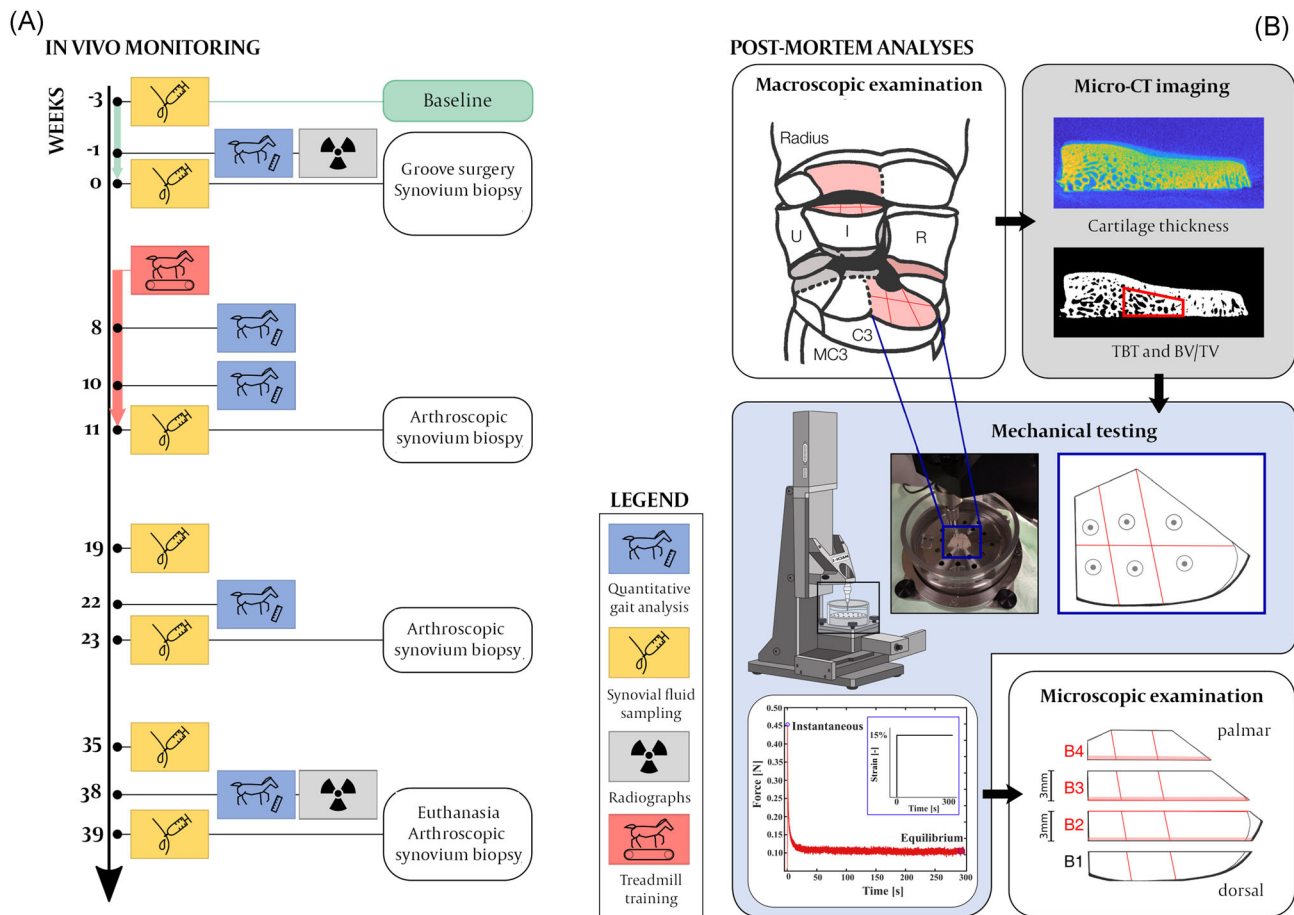


FIGURE 2 (A) Study design for in vivo monitoring. During the baseline period, ponies were accustomed to treadmill exercise. Groove surgery was performed through arthrotomy. (B) Workflow of post-mortem analyses [Color figure can be viewed at wileyonlinelibrary.com]

were evaluated using Fiji software (ImageJ, version 2.0.0-rc-69, <https://imagej.net>).

2.7 | Semi-automated mechanical indentation testing of cartilage

Measurement was done at three points dorsal and three points palmar of the groove running in mediolateral direction (Figure 2B). After thawing at room temperature, measurements were conducted using a Biomomentum Mach-1 v500css (Biomomentum Inc.) with a 70 N multiaxial load-cell and a nonporous spherical tip indenter ($d = 0.5$ mm, MA034; Biomomentum). Briefly, a one-step stress-relaxation protocol was implemented using a ramp rate of 100%/s, 15% (of the cartilage thickness) step and 300 s relaxation time.^{14–16} Equilibrium and instantaneous Young's moduli were calculated and corrected using Hayes equation¹⁷ (Supporting Information Text S4).

2.8 | Microscopic examination of cartilage

Osteochondral samples were cut at 6 mm from the (virtual) central groove towards the dorsal and palmar sides. They were fixated in 10%

formalin (Riedel-de Haen 33220) and decalcified in 0.5 M ethylenediaminetetraacetic acid (prod. 20296.360, VWR; Radnor) at pH 7.0 for 10 weeks. Samples were further divided into four parts and embedded in paraffin. Five micrometer thick sections from three locations per sample (directly adjacent to and at 3 mm from the central groove (Figure 2B) were stained with Safranin-O/Fast-green (SOFG), blind-coded, and graded at a 0–20 scale¹³ in randomized order by two observers (NM, SP). The proteoglycan (PG) depletion within a 1-mm rectangular region-of-interest (ROI) around each groove was determined based on optical density values from digital densitometry images (Supporting Information Text S5, Figure S1). Collagen type 1 and 2 immunohistochemistry was performed using collagen 1 rabbit monoclonal antibody (ab138492; Abcam) and collagen 2 mouse monoclonal antibody (II-II6B3, DSHB; Supporting Information Text S6).

2.9 | Radiographic analysis

Radiographs were taken bilaterally before and at 38 weeks after groove surgery, including the following views: lateromedial, flexed lateromedial, dorsopalmar, dorsomedial-palmarolateral and dorsolateral-palmaromedial oblique and dorsoproximal-dorsodistal oblique at 85° and 55°. Images were blind-coded and

radiocarpal and middle carpal joints were assessed separately for subchondral bone lysis, bone proliferation at the joint capsule attachment (enthesophytes), and osteophyte formation, each on a 0-3 scale,¹⁸ by one board-certified veterinary radiologist (MB).

2.10 | Synovial membrane microscopy

At each surgery, synovium biopsies from each joint were taken for histology and gene expression analysis. Samples for histology were fixed in formaldehyde solution 4% (Klinipath 4078.9005) and embedded in paraffin. Five- μ m thick sections were stained with hematoxylin-eosin, blind-coded, and graded on a 0-20 scale¹³ in randomized order by two observers (SP, NM).

2.11 | Synovial membrane quantitative polymerase chain reaction (qPCR)

For RNA isolation, the RNeasy Mini kit (QIAGEN) was used according to the manufacturer's guidelines. An input of 300 ng total RNA per sample was reverse-transcribed into complementary DNA (cDNA) and subsequently, SybrGreen quantitative real-time PCR (qRT-PCR) was performed (Supporting Information Text S7). Target genes included matrix metalloproteinase-3 (MMP-3), chemokine (C-C motif) ligand 2 (CCL2), interleukin-1 receptor (IL1R), interleukin-6 (IL-6), transforming growth factor- β 1 (TGF- β 1), activin receptor-like kinase-5 and -1 (ALK5 and ALK1), and plasminogen activator inhibitor-1 (Pai1) (Table S1). Five reference genes were selected (Supporting Information Text S7) and relative expression was calculated according to the normalized relative quantity (NRQ) method¹⁹ in Microsoft Excel (version 16.24). Statistically significant changes were considered relevant when fold-changes > 2.

2.12 | Synovial fluid composition

SF was collected into uncoated tubes before each surgery and additionally at weeks -3, 19, and 35. Before arthrocentesis, ponies were sedated with detomidine and butorphanol and the arthrocentesis area was aseptically prepared. Samples were processed within 30 min. Total nucleated cell count (TNC) and total protein (TP) concentration (hand-held refractometer; Euromex Holland) were measured, and predominant cell populations were identified by microscopic evaluation of rapid stained smears. Control samples from radiocarpal and middle carpal joints were averaged for analysis. The remainder of the sample was centrifuged (at 2520g for 5 min). The cell-free supernatant was transferred to 2 ml Eppendorf tubes and stored at -80°C for biomarker analysis.

Five biomarkers were evaluated in SF collected at week -3 (baseline), week 19, and week 35. Concentrations of type II collagen synthesis marker carboxypropeptide (CPII), type II collagen cleavage

(C2C) marker (Ibex; Montreal), and the inflammation and pain-related marker CC-chemokine ligand 2 (CCL2; KingFisherBiotech) were measured by commercial ELISA kits (Supporting Information Text S8). General MMP activity was measured using a fluorometric assay based on the cleavage of the fluorogenic peptide substrate FS-6.²⁰ Glycosaminoglycan (GAG) concentrations were measured using a modification of the 1,9-dimethylmethylene blue assay.²¹ Control samples from radiocarpal and middle carpal joints were pooled. Samples from grooved joints were pooled at baseline.

2.13 | Quantitative gait analysis

Optical motion capture data was collected by 18 high-speed infrared cameras (Oqus 700+, 200 Hz; Qualisys AB) 2 weeks before and at 8, 10, 22, and 38 weeks after groove surgery (Supporting Information Text S9). Symmetry parameters MaxDiff and MinDiff (i.e., differences between the two maxima and minima of vertical displacement, respectively) and range of motion were calculated for head, withers, and pelvis.²²

2.14 | Statistical analysis

R software (version 3.5.2) was used. Ordinal data (radiographic and macroscopic scores) were analyzed using Friedman testing with Tukey HSD post hoc comparison. A paired ttest was used for two-group comparisons (blunt vs. sharp) with continuous outcomes (optical density values). For more than two groups with continuous outcomes, linear mixed effect models were used with multiple fixed effects and with pony as random effect (nlme package, version 3.1-137), followed by pair-wise comparisons of estimated means with false discovery rate correction to test for differences between groups. Using these approaches, dependences within animals could be taken into account. Logarithmic or square root transformations were used when needed to meet the model assumptions (details in Table S2). Model fit was tested using Akaike's Information Criterion and presented model estimates were based on restricted maximum likelihood estimators. $p < 0.05$ was set as the limit of statistical significance. Macroscopic and microscopic scores of two observers were averaged for analysis. As a measure of interobserver agreement, the intraclass correlation coefficient (ICC) was calculated (two-way random model for agreement on single measurements).

3 | RESULTS

3.1 | Macroscopic and microscopic examination of the cartilage

Macroscopically, blunt grooves were clearly visible and showed a crumbling aspect at the edges of the grooves. Sharp grooves were hardly visible. In neither of the groove types, signs of defect filling were seen. In most samples from blunt-grooved joints, an imprint was seen at the

kissing site. The surfaces of both grooved and control joints showed mild to moderate degenerative changes (Figures 3 and S2A). The ICC (95% confidence interval [CI]) of two observers was 0.443 (−0.089 to 0.771).

Microscopically, blunt lesions typically reached to the calcified cartilage layer and caused detachment of the non-calcified cartilage at the tidemark. Big clusters (up to 19 cells) and loss of SOFG staining characterized the area adjacent to the lesions. Sharp lesions typically reached into the deep zone of the non-calcified cartilage and caused mild changes to the adjacent tissue (Figure 4). In two ponies, filling of blunt defects with fibrocartilage-like tissue was observed. In one of them this was also seen in a sharp defect (Figure 5). Estimated mean (95% CI) OARSI scores were higher in grooved samples compared with their controls (16.9 [15.7–18.1] vs. 10.2 [9.0–11.5] for blunt and 14.9 [13.7–16.2] vs. 11.2 [9.9–12.4] for sharp; $p < 0.0001$); this was not the case for the kissing sites (Figure S2B). Blunt-grooved samples scored significantly higher than sharp grooved samples ($p = 0.007$). The ICC (95% CI) of two observers was 0.902 (0.874–0.924). Normalized mean (\pm SD) optical density, as a measure of proteoglycan content, was significantly lower around blunt grooves than around sharp grooves (0.57 ± 0.21 and 0.92 ± 0.28 , resp.; $p = 0.006$). Qualitative evaluation of collagen staining showed collagen type 2 loss in the cartilage directly adjacent to the blunt lesions and, to a lesser extent, at the edges of sharp

lesions. Collagen type 1 staining was only (minimally) seen in the repair tissue found in two blunt-grooved samples (Figure 5).

3.2 | Micro-CT imaging of cartilage and subchondral bone

The estimated mean (95% CI) cartilage thickness opposite to the sharp grooves was higher than their contralateral controls in the middle carpal joint (471 [388–572] μm vs. 398 [328–483] μm ; $p = 0.005$). No other differences in cartilage thickness, mean trabecular thickness, or trabecular bone volume fraction were observed between grooved samples and their controls (Figure S3).

3.3 | Biomechanical measurements of cartilage

Biomechanical moduli trended lower in the grooved joints than in their controls (Figure 6).

For the equilibrium modulus the estimated mean (95% CI) was lower in the cartilage opposite blunt grooves in the middle carpal joint (0.73 [0.59–0.90] vs. 0.95 [0.77–1.14] MPa; $p = 0.021$) and in sharp grooved cartilage in the radiocarpal joint (0.86 [0.71–1.03] vs.

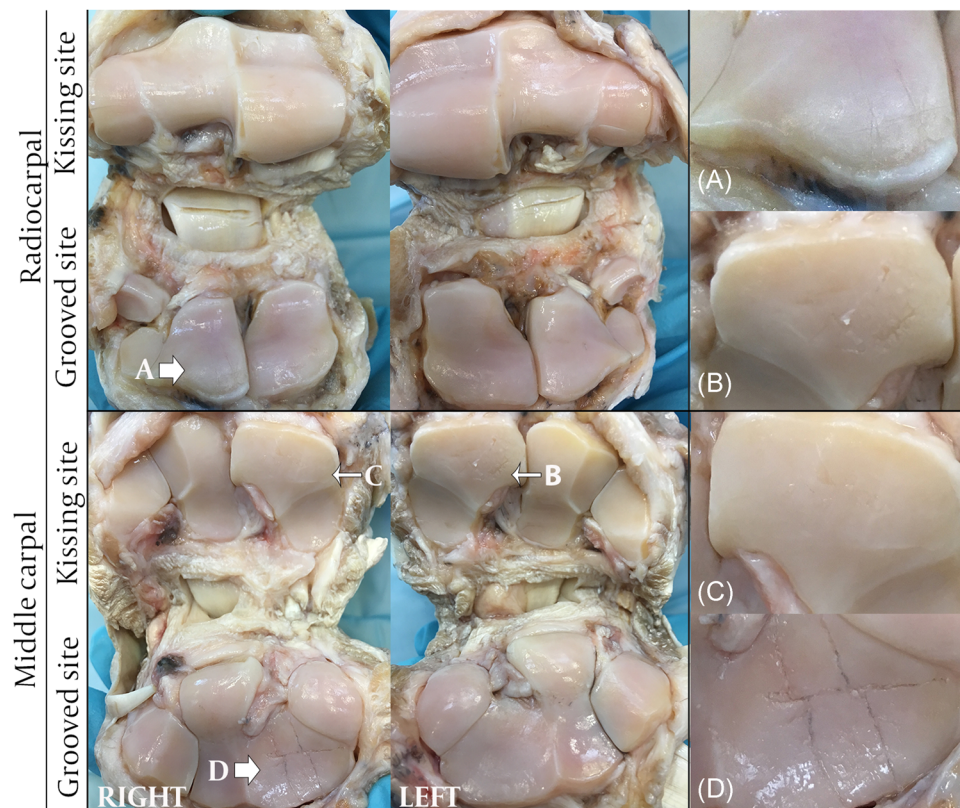


FIGURE 3 Gross appearance of the articular cartilage surface of grooved (left column = right limb) and sham-operated (middle column = left limb) joints of an individual at 39 weeks. Right column presents enlargements of the carpal bones labeled (A–D) in the left and middle columns. Sharp grooves (A) and blunt grooves (D) are present in the right joint. The kissing site in the left middle carpal joint shows a press-pattern of the blunt grooves (C). The kissing site in the right middle carpal joint shows a grade 3 lesion possibly resulting from the surgery (B) [Color figure can be viewed at wileyonlinelibrary.com]



FIGURE 4 Light microscopy images of articular cartilage sections with blunt and sharp grooves (pony 1-9). COLII/I, collagen type 2/1 immunohistochemistry staining; SOFG, Safranin-O Fast-Green staining. “reference” shows freshly made blunt and sharp lesions in a cadaver joint [Color figure can be viewed at wileyonlinelibrary.com]

1.10 [0.93–1.30] MPa; $p = 0.009$). The instantaneous modulus was lower in both blunt- and sharp-grooved cartilage in the radiocarpal joint (6.42 [4.56–8.59] vs. 8.39 [6.22–10.9] MPa; $p = 0.021$, and 5.64 [4.13–7.39] vs. 6.93 [5.23–8.88] MPa; $p = 0.045$, respectively).

3.4 | Radiographic analysis

No statistically significant changes in radiographic scores were seen. The biggest increase of mean (\pm SD) scores was observed in

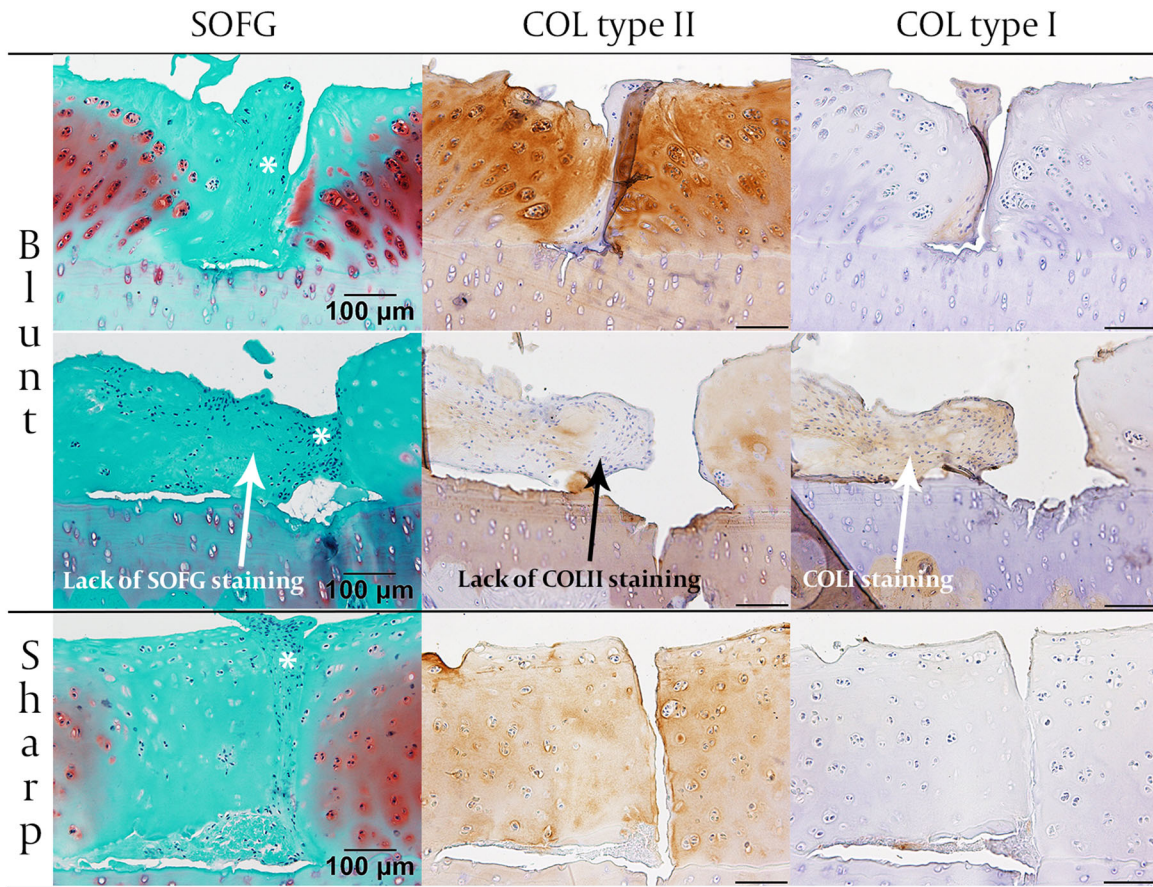


FIGURE 5 Light microscopy images of articular cartilage sections with fibro-cartilage-like filling of blunt (ponies 5 and 9, respectively) or sharp (pony 9) grooves. White asterisk indicates fibro-cartilage-like tissue. Lack of collagen type 2 staining and positive staining for collagen type 1 was observed in the blunt grooves. The fibro-cartilage-like tissue observed in the SOFG-stained section of the sharp groove, was not found in the collagen type 1 and 2-stained sections [Color figure can be viewed at wileyonlinelibrary.com]

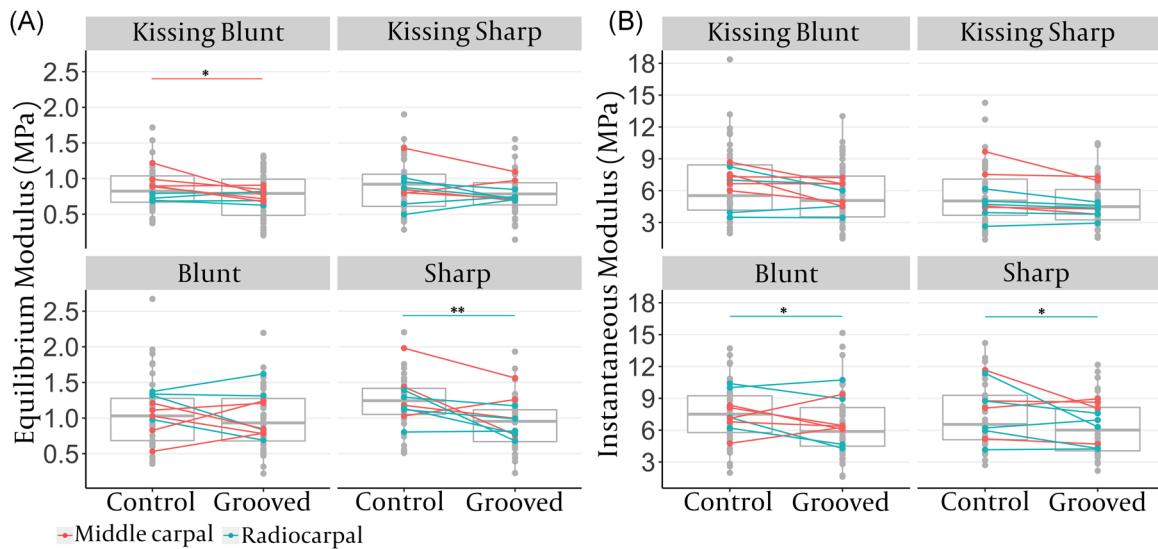


FIGURE 6 Post-mortem cartilage biomechanical properties. Spaghetti plots show cartilage equilibrium modulus (A) and instantaneous modulus (B) per pony averaged over six measured locations. Gray boxplots represent medians with interquartile ranges of all measured locations (gray dots). * $p < 0.05$; ** $p < 0.01$ [Color figure can be viewed at wileyonlinelibrary.com]

blunt- (0 [0]–1.8 [1.3]) and sharp-grooved (0 [0]–1.4 [1.3]) radiocarpal joints (Table S3 and Figure S4).

3.5 | Synovial membrane microscopy

A total number of 138/144 of synovium sections was graded (four controls, one blunt, and one sharp were excluded due to insufficient quality). Treatment groups could not be distinguished statistically at any time point (Figure S5). The ICC (95% CI) of two observers was 0.759 (0.678–0.822).

3.6 | Synovial membrane quantitative PCR

A mean (\pm SD) RNA yield of 35.5 (\pm 26.1) ng/ μ l was obtained. Eight samples (four controls, two blunt, and two sharp) were excluded because of poor RNA quality or because C_t values were out of the detection range. Measures of qPCR quality are provided in Table S4. Expression levels of interleukin-6 (IL-6) were higher in grooved joints than in their contralateral controls at week 23 ($p = 0.042$). The estimated mean (95% CI) NRQ in blunt-grooved joints was 4.27 (1.16–15.7) versus 1.38 (0.32–5.93) in their controls. For the sharp group this was 4.99 (1.36–18.3) versus

0.69 (0.19–2.53). Expression levels of IL-6, CCL2, and ALK5 showed increases over time that were statistically significant and relevant only in grooved joints. Changes in expression levels in other markers were observed over the level of treatment group only (Figure S6).

3.7 | Synovial fluid

TNC could not be measured in 3/216 samples (two blunt grooved and one control) due to a technical error. Total protein levels remained within a clinically normal range (0–3 g/dl) and therefore, the time-related decrease was not considered relevant. The estimated mean (95% CI) TNC increased over the level of treatment group from 0.33 (0.18–0.61) G/L at baseline to 5.20 (2.84–9.56) G/L at week 39 ($p < 0.0001$), with a small peak of 2.40 G/L at week 11 (95% CI 1.29–4.44; $p < 0.0001$). This could be explained by an increasing presence of lymphocytes (Table S5).

In SF extracted from blunt-grooved joints, the estimated mean (95% CI) CPII/C2C ratio increased significantly from 5.84 (4.10–7.90) at baseline to 9.16 (6.80–11.9) at week 35, reaching a higher level than sharp-grooved (5.59 [3.78–7.75], $p = 0.0075$) and control joints (6.3 [4.37–8.58], $p = 0.0248$) at that point. For GAG and MMP analysis 1/72 samples and for CCL2 analysis 3/72 samples (blunt) could not be measured due to limited material. For these

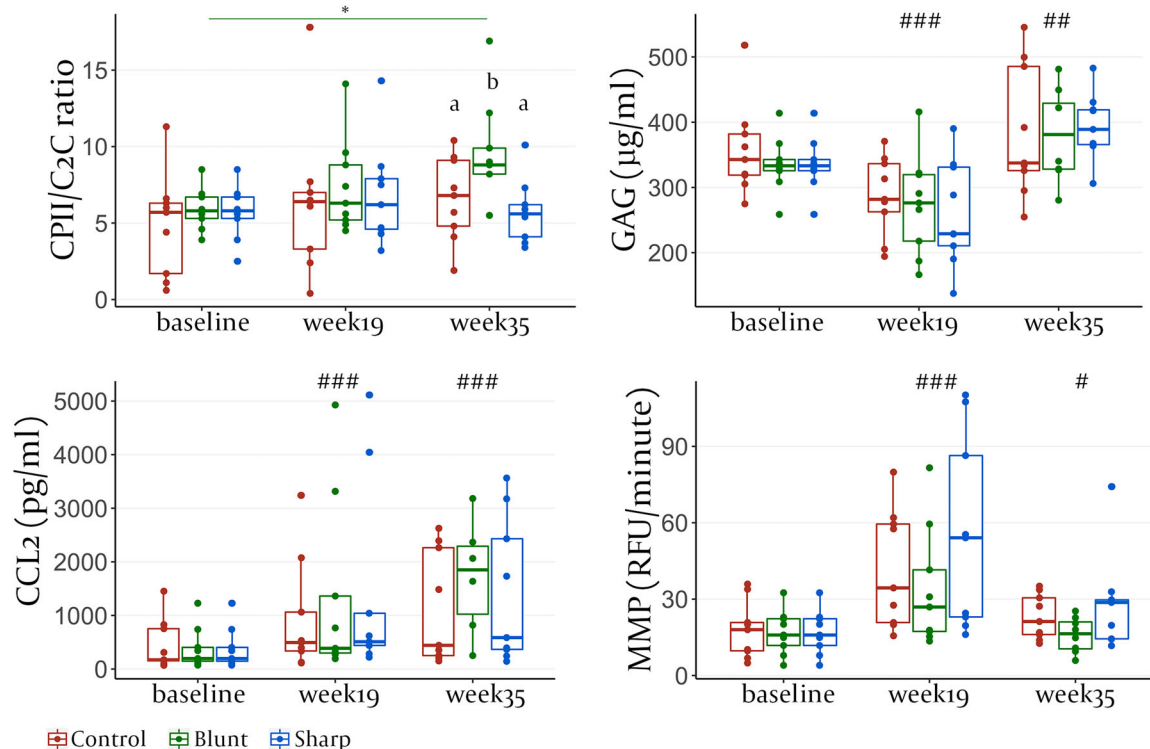


FIGURE 7 Biomarkers in synovial fluid. Medians (\pm interquartile ranges) of CII/C2C ratio, glycosaminoglycan (GAG) and chemokine (C-C motif) ligand 2 (CCL2) concentrations, and matrix metalloproteinase (MMP) activity in synovial fluid from control joints and blunt- and sharp-grooved joints. *Significant differences between time points, within treatment group. #Significant differences with baseline for all treatment groups. */# $p < 0.05$; **/## $p < 0.01$; ***/### $p < 0.001$. Treatment groups with non-corresponding letters are significantly different [Color figure can be viewed at wileyonlinelibrary.com]

markers, time-related changes occurred over the level of treatment group only (Figure 7).

3.8 | Quantitative gait analysis

One pony was withdrawn from treadmill training after 5 weeks and excluded from gait analysis because of recurrent mild lameness (1–2/5), related to mild desmopathy of the interosseous tendon branches and bilateral shoulder OA. The estimated mean (95% CI) absolute MinDiff of the head gradually increased, reaching a maximum of 14.8 (12.2–17.3) mm at week 22 (vs. 8.43 [6.23–10.6] mm at baseline; $p < 0.0001$). No further statistically significant or clinically relevant changes in symmetry were found. The range of motion of the head decreased on the short term (–6.4 mm at week 8) but increased on the long term (+4 mm at week 38). For the withers and pelvis, a decrease in range of motion was seen over the long term (Table S6).

4 | DISCUSSION

In this model, both blunt and sharp cartilage grooves led to a certain degree of degeneration in the adjacent articular cartilage, as evidenced by significantly higher OARSI scores of grooved cartilage, compared with the contralateral controls. Blunt lesions resulted in more extensive proteoglycan depletion and loss of collagen type 2 staining, and more pronounced cluster formation and focal cell loss. There were no relevant differences in cartilage thickness, but cartilage biomechanical moduli were lower in grooved joints, indicating less-than-normal resilience. Concomitant changes in other joint tissues remained limited to higher IL-6 expression levels in synovium at week 23 and an increased CPII/C2C ratio in SF from blunt-grooved joints at week 35.

The features of blunt and sharp grooves in this study were similar to those described in previous *in vivo* models.^{4–7,10,23,24} However, despite macroscopically visible imprints of particularly blunt grooves, kissing sites were not assigned higher OARSI scores than contralateral controls, as described in sheep and rats.^{5,6} This could be due to the repeated arthrocentesis and joint surgeries which may have caused unintended damage, leveling out the difference in degeneration scores. Additionally, we found fibro-cartilage-like tissue in some defects in two individuals. This has not been reported in other groove models, but partial defect filling with fibrous repair tissue has been described in the equine carpus, 3 months²⁵ and 1 year²⁶ after the creation of a chondral lesion. The fact that we observed this only in some individuals may highlight the variation in individual responses to cartilage damage. An *in vitro* study comparing blunt and sharp trauma in immature bovine cartilage explants reported a band of cell death adjacent to the blunt lesion edge extending approximately 100 μ m into the tissue and viable cells immediately adjacent to the edge of sharp lesions. Also, loss of safranin-O staining at the

edge of blunt lesions extended further into the tissue. It was hypothesized that there is less initial disruption of the matrix and less mechanical stress immediately adjacent to the edge of a sharp defect.^{11,27}

Interestingly, the lower cartilage stiffness around the grooves than in controls was only significant in the radiocarpal joints. This could be related to a higher range of motion and different contributions of shear and compression to the total forces than in the middle carpal joints.²⁸ The bigger changes in radiographic scores observed in grooved radiocarpal joints than middle carpal joints may support this theory. Possibly, changes would have been greater if indentation had been performed closer to the grooves than at 2 mm, a value chosen to minimize edge effects.²⁹ Digital densitometry (reflecting fixed charged density of proteoglycans, which strongly influences the equilibrium modulus¹²) showed reduced optical density values mostly within less than a 1 mm rectangular ROI around the grooves.

The cartilage defects produced an upregulated IL-6 expression at week 23. Immunostaining of the synovium or analysis of IL-6 concentration in SF may confirm whether this resulted in an actually increased IL-6 production. The time-related increases in IL-6, CCL2 and ALK5 expression in grooved joints only suggest that cartilage damage may enhance gene transcription. The higher SF CPII/C2C ratio in blunt-grooved joints versus sharp-grooved and control joints at week 35, suggests a locally upregulated collagen turnover. In previous equine chondral defect models, no differences in SF biomarker concentrations between traumatized and sham-operated joints were found,^{7,30} but significant differences were present when the defect included the subchondral bone.³¹ Mean thickness of the trabeculae or bone volume fraction were not different between grooved and control joints at week 39, which is in line with previous findings in sheep and dogs.^{5,32} However, changes may have taken place at an earlier phase, following the theory of biphasic bone remodeling.³² Furthermore, subtle changes to the subchondral bone plate or calcified cartilage layer cannot be excluded based on the current data.

However, a pilot study with Fourier transform infrared microspectroscopy showed a decreased mineralization in both layers of blunt grooved samples ($n = 6$) compared with controls ($n = 5$).³³ No direct effect on gait quality of cartilage lesions was measured. Previous groove model studies reported gait changes within 10 weeks after surgery.^{7,34} The overall gradually increasing absolute MinDiff values of the head together with the increased range of motion of the head on the longer term (week 38) are indicative of a mildly progressive lameness.³⁵

We monitored groove-related changes over a period of 9 months with each individual serving as its own control. This helped decrease the number of experimental animals and the degree of biological variation between them, but also brought limitations. Sham-operated control joints were not entirely free from cartilage lesions and surgeries and serial SF and synovium sampling likely induced bilateral inflammatory responses that may have been partly responsible for the time-related changes

observed independent of treatment.³⁶⁻³⁸ Another potential confounder is exercise (i.e., mechanical loading), which can influence joint homeostasis through various mechanisms.³⁹ This tallies well with the changes in synovium gene expression and SF biomarkers, irrespective of the treatment group. Together, these factors may have minimized the differences between grooved and control joints. Furthermore, the study design did not allow for time-dependent histopathological assessment of the articular cartilage. However, longitudinal evaluation of the cartilage was performed using arthroscopic near-infrared spectroscopy.⁴⁰ A long-term contribution to early pathobiological events of OA cannot be excluded, but the direct effect of blunt or sharp cartilage damage on joint homeostasis appeared limited. Therefore, cartilage damage in itself may not be too important, as long as the tissue's biomechanical function remains sufficient. This observation is in line with the well-known lack of relationship between the extent of cartilage lesions and clinical manifestation of OA and the often huge time lag between initial cartilage damage and the clinical presentation of OA.⁴¹ However, lesion progress is slow but inevitable. The combination of lesion size and morphology, together with the loading profile, will still determine progress and hence probably the moment when these lesions do become clinically important. The role of inflammation seemed rather limited in the current study, but the upregulation of IL-6 and CCL2 expression in the synovium may provide clues to further investigation.

In the search for leads to improve timely recognition and treatment of OA, longer follow-up (several years) may be needed to bring about measurable effects of minor cartilage damage on joint homeostasis. However, such studies are practically very demanding, expensive, and bear ethical considerations. Quicker progress of degeneration may be achieved with more extensive grooves or using high motion joints that are subjected to more shear forces than the carpal joint. However, the question as to what extent quick and short-term models mimic the natural situation as encountered in the human or equine clinic, and therefore their translational value, remains a point of discussion. Higher sensitivity techniques like proteomics and metabolomics could contribute to more adequate profiling of synovial tissues⁴²⁻⁴⁴ and might be able to pick up changes not detected with the current methods. The interplay between the morphology of the lesion, degree of tissue disruption, mechanical loading, and inflammatory responses, could be further studied by *in vivo* mechanical testing and computational modeling.^{12,45} Data obtained by *in vivo* studies like ours, is of great value for the validation of such models.

In conclusion, sharp and blunt grooves in the non-calcified cartilage layer of the equine carpal joint, do not repair. Microscopic observations and biomechanical data showed that the reaction of the tissue adjacent to the defect varies dependent on the characteristics of the lesion. The overall effect of minor cartilage lesions on joint homeostasis and clinical presentation is limited, but they irrevocably cause a certain degree of degeneration. It is likely that it is the combination of lesion size and configuration, together with the

loading profile that will determine the speed and character of further degeneration.












ACKNOWLEDGMENTS

This study was made possible by an NWO Graduate Programme Grant (022.005.018), support from Dutch Arthritis Association grant LLP-22, and the University of Eastern Finland's Doctoral Programme in Science, Technology and Computing (SCITECO). Funding sources had no role in the design of the study, analysis, and interpretation of the results, or writing and submission of the manuscript for publication. Alekski Leinonen and Dr. Rubina Shaikh are acknowledged for logistic support and their contribution to sample processing for histology. Furthermore, we thank Eija Rahunen for technical assistance in histology, Dristi Regmi and Mohammedhossein Ebrahimi for assistance in digital densitometry analysis, Hans Vernooij for statistical advice, and Emmie Giessen and Angelica Enström for their assistance in training, surgeries and SF collection.

AUTHOR CONTRIBUTIONS

Contributed to the overall conception and design of the study: Nikae C.R. te Moller, Harold Brommer, and P. René van Weeren. *Contributed to conception and design of micro-CT and biomechanical measurements:* Ali Mohammadi, Behdad Pouran, Janne T.A. Mäkelä, Rami K. Korhonen, and Juha Töyräs. *Contributed to collection and assembly of data:* Nikae C.R. te Moller, Ali Mohammadi, Saskia Plomp, Filipe M. Serra Bragança, Martijn Beukers, Behdad Pouran, Isaac O. Afara, Ervin Nippolainen, and Harold Brommer. *Contributed to analysis and/or interpretation of the data:* Nikae C.R. te Moller, Ali Mohammadi, Filipe M. Serra Bragança, Janne T.A. Mäkelä, Rami K. Korhonen, and P. René van Weeren. *Contributed to the statistical analysis:* Nikae C.R. te Moller and Filipe M. Serra Bragança. *Provided ample technical and logistic support:* Saskia Plomp. *Contributed to drafting of the article:* Nikae C.R. te Moller and Ali Mohammadi. All authors revised the article and approved the final manuscript. Responsibility for the integrity of the work as a whole, from inception to finished article is taken by NM (n.c.r.temoller@uu.nl) and RW (r.vanweeren@uu.nl).

ORCID

Nikae C. R. te Moller  <http://orcid.org/0000-0001-8675-330X>
 Ali Mohammadi  <http://orcid.org/0000-0001-6254-0879>
 Filipe M. Serra Bragança  <https://orcid.org/0000-0001-8514-7949>
 Martijn Beukers  <https://orcid.org/0000-0003-0866-8286>
 Isaac O. Afara  <https://orcid.org/0000-0001-7114-0439>
 Ervin Nippolainen  <https://orcid.org/0000-0002-1317-2683>
 Janne T. A. Mäkelä  <http://orcid.org/0000-0002-6123-1262>
 Rami K. Korhonen  <http://orcid.org/0000-0002-3486-7855>
 Juha Töyräs  <https://orcid.org/0000-0002-8035-1606>
 Harold Brommer  <https://orcid.org/0000-0002-3622-8571>
 P. René van Weeren  <https://orcid.org/0000-0002-6654-1817>

REFERENCES

1. Penell JC, Egenvall A, Bonnett BN, Olson P, Pringle J. Specific causes of morbidity among Swedish horses insured for veterinary care between 1997 and 2000. *Vet Rec.* 2005;157(16):470-477.
2. McIlwraith CW, Fortier LA, Frisbie DD, Nixon AJ. Equine models of articular cartilage repair. *Cartilage.* 2011;2(4):317-326.
3. Malda J, Benders KEM, Klein TJ, et al. Comparative study of depth-dependent characteristics of equine and human osteochondral tissue from the medial and lateral femoral condyles. *Osteoarthr Cartil* 2012;20:1147-1151.
4. Marijnissen ACA, van Roermund PM, Verzijl N, Tekoppele JM, Bijlsma JWJ, Lafeber FPJG. Steady progression of osteoarthritic features in the canine groove model. *Osteoarthr Cartil* 2002;10(4):282-289.
5. Mastbergen SC, Pollmeier M, Fischer L, Vianen ME, Lafeber FPJG. The groove model of osteoarthritis applied to the ovine fetlock joint. *Osteoarthr Cartil.* 2008;16(8):919-928.
6. de Visser HM, Weinans H, Coeleveld K, van Rijen MH, Lafeber FP, Mastbergen SC. Groove model of tibia-femoral osteoarthritis in the rat. *J Orthop Res.* 2016;24:S400-S401.
7. Maninchedda U, Lepage OM, Gangl M, et al. Development of an equine groove model to induce metacarpophalangeal osteoarthritis: a pilot study on 6 horses. *PLOS One.* 2015;10(2):e0115089.
8. te Moller NCR, Brommer H, Plomp S, van Weeren PR. Development of an equine carpal groove model to study early changes in osteoarthritis—a pilot study. *Osteoarthr Cartil* 2018;26(Suppl 1):S132-S133.
9. Malda J, Groll J, van Weeren PR. Rethinking articular cartilage regeneration based on a 250-year-old statement. *Nat Rev Rheumatol.* 2019;15(10):571-572.
10. Meachim G. The Effect of scarification on articular cartilage in the rabbit. *J Bone Joint Surg Br.* 1963;45(1):150-161.
11. Redman SN, Dowthwaite GP, Thomson BM, Archer CW. The cellular responses of articular cartilage to sharp and blunt trauma. *Osteoarthr Cartil.* 2004;12(2):106-116.
12. Orozco GA, Tanska P, Florea C, Grodzinsky AJ, Korhonen RK. A novel mechanobiological model can predict how physiologically relevant dynamic loading causes proteoglycan loss in mechanically injured articular cartilage. *Sci Rep.* 2018;8(1):15599.
13. McIlwraith CW, Frisbie DD, Kawcak CE, Fuller CJ, Hurtig M, Cruz A. The OARSI histopathology initiative—recommendations for histological assessments of osteoarthritis in the horse. *OAC Histopathol Suppl.* 2010;18:S93-S105.
14. Ebrahimi M, Ojanen S, Mohammadi A, et al. Elastic, viscoelastic and fibril-reinforced poroelastic material properties of healthy and osteoarthritic human tibial cartilage. *Ann Biomed Eng.* 2019;47:953-966.
15. Mäkelä JTA, Han SK, Herzog W, Korhonen RK. Very early osteoarthritis changes sensitively fluid flow properties of articular cartilage. *J Biomech.* 2015;48(12):3369-3376.
16. Mäkelä JTA, Rezaeian ZS, Mikkonen S, et al. Site-dependent changes in structure and function of lapine articular cartilage 4 weeks after anterior cruciate ligament transection. *Osteoarthr Cartil.* 2014;22(6):869-878.
17. Hayes WC, Keer LM, Herrmann G, Mockros LF. A mathematical analysis for indentation tests of articular cartilage. *J Biomech.* 1972;5(5):541-551.
18. Kawcak CE, Frisbie DD, McIlwraith CW, Werpy NM, Park RD. Evaluation of avocado and soybean unsaponifiable extracts for treatment of horses with experimentally induced osteoarthritis. *Am J Vet Res.* 2007;68(6):598-604.
19. Hellemans J, Mortier G, De Paepe A. qBase relative quantification framework and software for management and automated analysis of real-time quantitative PCR data. *Genome Biol.* 2007;8(2):R19.
20. Neumann U, Kubota H, Frei K, Ganu V, Leppert D. Characterization of Mca-Lys-Pro-Leu-Gly-Leu-Dpa-Ala-Arg-NH₂, a fluorogenic substrate with increased specificity constants for collagenases and tumor necrosis factor converting enzyme. *Anal Biochem.* 2004;328(2):166-173.
21. Farndale RW, Buttle DJ, Barrett AJ. Improved quantitation and discrimination of sulphated glycosaminoglycans by use of dimethylmethylene blue. *Biochim Biophys Acta.* 1986;883(2):173-177.
22. Rhodin M, Roepstorff L, French A, Keegan KG, Pfau T, Egenvall A. Head and pelvic movement asymmetry during lungeing in horses with symmetrical movement on the straight. *Equine Vet J.* 2016;48(3):315-320.
23. Forney HJ, Bentley G, Mathews RS. Salicylates and repair in adult articular cartilage: a preliminary report. *Orthop Oxf* 1973;6(1):19-31.
24. Simmons DP, Chrisman DO. Salicylate inhibition of cartilage degeneration. *Arthritis Rheum.* 1965;8(5):960-969.
25. French DA, Barber SM, Leach DH, Doige CE. The effect of exercise on the healing of articular cartilage defects in the equine carpus. *Vet Surg.* 1989;18(4):312-321.
26. Saloniemi E, Rieppo L, Nissi MJ, et al. Critical-sized cartilage defects in the equine carpus. *Connect Tissue Res.* 2019;60(2):95-106.
27. Tew SR, Kwan APL, Hann A, Thomson BM, Archer CW. The reactions of articular cartilage to experimental wounding: role of apoptosis. *Arthritis Rheum.* 2000;43(1):215-225.
28. Smyth PA, Rifkin RE, Jackson RL, Reid Hanson R. The fractal structure of equine articular cartilage. *Scanning.* 2012;34(6):418-426.
29. Spilker RL, Suh J-K, Mow VC. A finite element analysis of the indentation stress-relaxation response of linear biphasic articular cartilage. *J Biomech Eng.* 1992;114(2):191-201.
30. Niemelä TM, Tulamo R-M, Carmona JU, López C. Evaluation of the effect of experimentally induced cartilage defect and intra-articular hyaluronan on synovial fluid biomarkers in intercarpal joints of horses. *Acta Vet Scand.* 2019;61(1):24.
31. Frisbie DD, Al-Sobayil F, Billinghurst RC, Kawcak CE, McIlwraith CW. Changes in synovial fluid and serum biomarkers with exercise and early osteoarthritis in horses. *Osteoarthr Cartil.* 2008;16(10):1196-1204.
32. Intema F, Sniekers YH, Weinans H, et al. Similarities and discrepancies in subchondral bone structure in two differently induced canine models of osteoarthritis. *J Bone Miner Res.* 2010;25(7):1650-1657.
33. Turunen MJ, Moller NCR, Nippolainen E, et al. 2019. Compositional changes in subchondral bone and calcified cartilage in an equine cartilage defect model—A pilot study. In: ECSBM. Dublin, Ireland.
34. Frost-Christensen LN, Mastbergen SC, Vianen ME, et al. Degeneration, inflammation, regeneration, and pain/disability in dogs following destabilization or articular cartilage grooving of the stifle joint. *Osteoarthr Cartil.* 2008;16(11):1327-1335.
35. Keegan KG, Wilson DA, Smith BK, Wilson DJ. Changes in kinematic variables observed during pressure-induced forelimb lameness in adult horses trotting on a treadmill. *Am J Vet Res.* 2000;61(6):612-619.
36. Boom R, Brama PAJ, Kiers GH, Degroot J, Barneveld A, Weeren PR. The influence of repeated arthrocentesis and exercise on matrix metalloproteinase and tumour necrosis factor activities in normal equine joints. *Equine Vet J.* 2004;36(2):155-159.
37. Lamprecht ED, Williams CA. Biomarkers of antioxidant status, inflammation, and cartilage metabolism are affected by acute intense exercise but not superoxide dismutase supplementation in horses. *Oxid Med Cell Longev.* 2012;2012:1-15.
38. Salazar-Noratto GE, De Nijs N, Stevens HY, Gibson G, Guldberg RE. Regional gene expression analysis of multiple tissues in an experimental animal model of post-traumatic osteoarthritis. *Osteoarthr Cartil.* 2019;27(2):294-303.

39. te Moller NCR, van Weeren PR. How exercise influences equine joint homeostasis. *Vet J*. 2017;222:60-67.
40. Sarin JK, te Moller NCR, Mohammadi A, Prakash M, Tornainen Jari, Brommer H, Nippolainen E, Shaikh R, Mäkelä JTA, Korhonen RK, van Weeren PR, Afara IO, Töyräs J. Machine learning augmented near-infrared spectroscopy: In vivo follow-up of cartilage defects. *Osteoarthritis and Cartilage*. 2020. <https://doi.org/10.1016/j.joca.2020.12.007>
41. Houck DA, Kraeutler MJ, Belk JW, et al. Do focal chondral defects of the knee increase the risk for progression to osteoarthritis? A review of the literature. *Orthop J Sport Med*. 2018;6(10):2325967118801931.
42. Anderson JR, Phelan MM, Clegg PD, Peffers MJ, Rubio-Martinez LM. Synovial fluid metabolites differentiate between septic and nonseptic joint pathologies. *J Proteome Res*. 2018;17(8):2735-2743.
43. Peffers MJ, McDermott B, Clegg PD, Riggs CM. Comprehensive protein profiling of synovial fluid in osteoarthritis following protein equalization. *Osteoarthr Cartil*. 2015;23(7):1204-1213.
44. Adams SB, Setton LA, Kensicki E, Bolognesi MP, Toth AP, Nettles DL. Global metabolic profiling of human osteoarthritic synovium. *Osteoarthr Cartil*. 2012;20(1):64-67.
45. Peloquin JM, Elliott DM. A comparison of stress in cracked fibrous tissue specimens with varied crack location, loading, and orientation using finite element analysis. *J Mech Behav Biomed Mater*. 2016;57:260-268.

SUPPORTING INFORMATION

Additional Supporting Information may be found online in the supporting information tab for this article.

How to cite this article: te Moller NCR, Mohammadi A, Plomp S, et al. Structural, compositional, and functional effects of blunt and sharp cartilage damage on the joint: A 9-month equine groove model study. *J Orthop Res*. 2021;39:2363-2375. <https://doi.org/10.1002/jor.24971>